Intra-event spatial correlation models for CAV and Arias Intensity based on regional site conditions

Wenqi Du & Gang Wang
Hong Kong University of Science and Technology, Hong Kong SAR, China

SUMMARY:
Spatial correlation models for ground motion intensity measures (IMs) are essential for seismic analysis of spatially distributed systems. In this paper, geostatistical analysis is conducted to calculate the spatial correlation for Cumulative Absolute Velocity (CAV) and Arias Intensity (Ia) using strong-motion data from nine recent earthquakes occurred in Taiwan, Japan and California. The results indicate that the spatial correlations for CAV and Ia are closely related to the regional site conditions, and they can be predicted based on the spatial correlations of V_{s30}. Due to their intrinsic similarity, CAV and Ia have similar spatial correlation coefficients. The results are also compared with spatial correlations of peak ground acceleration (PGA). It is also emphasized that correction methods are employed to eliminate artificial correlations due to biased distance scaling and V_{s30} estimation. Finally, an example is presented to demonstrate that the annual frequency of exceedance curves for spatially distributed IMs differ significantly if different ranges of spatial correlations are used .

Keywords: Spatial correlation, Arias Intensity, CAV, PGA, Regional site condition

1. INTRODUCTION

Considering spatial distribution of ground motion intensity measures (IM) is critical for seismic hazard analysis of spatially distributed infrastructure systems such as long-span bridges, lifelines, railways or geohazards. Traditional ground motion prediction equations (GMPEs) usually provide the statistical characteristics of IMs at a particular location for a casual earthquake event. However, the statistical characteristics of IMs at spatially separated locations are often overlooked. In recent years, spatial correlations of some important IMs such as the peak ground acceleration (PGA) and spectral acceleration (Sa) have been developed by several researchers (e.g., Boore *et al.*, 2003; Jayaram and Baker, 2009; Goda and Atkinson, 2010; Esposito and Iervolino, 2011). However, some other important IMs, like Cumulative Absolute Velocity (CAV) and Arias Intensity (Ia), have not yet been thoroughly studied.

CAV has been found to be a good index related to structural damages (EPRI, 1988). CAV is defined as the time integration of absolute acceleration as follows:

$$CAV = \int_0^{t_{tot}} \left| a(t) \right| dt \tag{1.1}$$

where $\left| a(t) \right|$ is the absolute value of the acceleration time history, and t_{tot} is the total duration of the ground motion time history. Similar to CAV, Arias Intensity (Arias, 1970) is the integration of the square of ground motion acceleration history over the total duration, given by the following equation:

$$Ia = \frac{\pi}{2g} \int_0^{t_{tot}} a(t)^2 \, dt \tag{1.2}$$

where g is the acceleration of gravity. By definition, CAV and Ia share intrinsic similarity in that they both incorporate the cumulative effect of an acceleration time history. Hence they can capture multiple characteristics of ground motion, including the amplitude, the frequency content and duration of the ground motion time histories in an implicit way.

Despite the fact that CAV and Ia have been regarded as promising IMs for seismic hazard evaluation, there are few spatial correlation models available. Most recently, Piggott and Stafford (2011) provided spatial correlation models of Ia based on ground motion data from the Northridge and Chi-Chi earthquakes. They found that it is not executable to provide a generic spatial correlation model since the spatial correlations differ significantly for these two events. To the best of the authors' knowledge, no spatial correlation model for CAV is available in literature.

In this study, recorded strong-motion data from nine recent earthquakes occurred in Taiwan, Japan and California are systematically compiled to evaluate the spatial correlation of CAV and Ia. The abundance of data enables development of an empirical model for estimating the spatial correlations based on regional site conditions. In order to calculate the intra-event residuals, the ground motion prediction equation for CAV proposed by Campbell and Bozorgnia (2010) (termed as CB10) and prediction equation for Ia by Campbell and Bozorgnia (2012) (termed as CB12) are chosen.

2. SPATIAL CORRELATION MODEL

Ground motion prediction equations (GMPEs) typically assume that IMs follow lognormal distribution. The observed logarithmic IM, denoted as $\ln Y_{ij}$, of a ground motion record can be written as follows:

$$\ln Y_{ij} = \overline{\ln Y_{ij}\left(M, R, \theta\right)} + \eta_i + \varepsilon_{ij} \tag{2.1}$$

where Y_{ij} is the ground motion IM of the j_{th} record of the i_{th} earthquake event, and $\overline{\ln Y_{ij}\left(M, R, \theta\right)}$ is the predicted median value of for $\ln Y_{ij}$ based on the magnitude (M), rupture distance (R) and other parameters (θ) of the event. The random variable η_i and ε_{ij} represent the inter-event and intra-event residuals, which are both assumed to be independent normally distributed with zero means and standard deviations of τ and σ, respectively. The standard deviation of the total residual term can be calculated by $\sigma_T = \sqrt{\sigma^2 + \tau^2}$, and then $\ln Y_{ij} = N\left(\overline{\ln Y_{ij}}; \sigma_T\right)$.

For a given earthquake event, the inter-event residual η_i is identical for all sites while the value of ε_{ij} varies with different sites (Abrahamson and Youngs, 1992). So, the total spatial correlation can be expressed as:

$$\rho_T\left(h\right) = \frac{\tau^2 + \rho_\varepsilon\left(h\right) \times \sigma^2}{\tau^2 + \sigma^2} \tag{2.2}$$

where $\rho_\varepsilon\left(h\right) = \rho_{\varepsilon_{i,j1};\varepsilon_{i,j2}}\left(h\right)$ represents the empirical spatial correlation obtained from intra-event residuals ε_{ij}, which is a function of the separation distance h between different sites. Given that the values of τ and σ are provided by GMPEs, estimation of $\rho_\varepsilon\left(h\right)$ is much more important. So in this paper we just focus on the study of $\rho_\varepsilon\left(h\right)$.

2.1. Estimation of empirical semivariogram

Semivariogram is a useful tool widely used to estimate the empirical spatial correlation of IMs. In general, the semivariogram $\gamma(\boldsymbol{h})$ measures the average dissimilarity between data separated by a vector $\boldsymbol{h}$. Under the assumptions that the spatial correlation is isotropic and second-order stationary, a scalar variable $h = \|\boldsymbol{h}\|$ can be used in the empirical semivariogram formulation:

$$\gamma(h) = \frac{1}{2} Var\left[z_{u_i+h} - z_{u_i} \right] = Var(z)\left[1 - \rho_{\varepsilon}(h)\right] \tag{2.3}$$

where z_{u_i} is a random distributed variable (in this paper, z_{u_i} refers to the intra-event residual ε_{ij} in Equation (2.1)) at position u_i and *h* again is the site-to-site separation distance (Cressie, 1993).

As an estimate of the theoretical semivariogram, the empirical semivariogram can be calculated from a sample dataset using estimators. A robust estimator is less sensitive to outliers, and it is defined as (Cressie, 1980):

$$\tilde{\gamma}(h) = \frac{\left(\frac{1}{N(h)} \sum_{i=1}^{N(h)} \left| z_{u_i+h} - z_{u_i} \right|^{0.5} \right)^4}{0.914 + 0.988 / N(h)} \tag{2.4}$$

where $\tilde{\gamma}$ represents empirical data, $N(h)$ is the number of pairs of sites separated by distance *h*. There are also some rules to properly define the size of the distance bins. It has been proposed that size of the bin should be no larger than a half of the maximum distance, and each bin contains at least 30 pairs of data.

2.2. Parametric fitting function

A parametric fitting function is useful to represent the empirical semivariogram. Exponential model has distinct advantage of simplicity, therefore, it is adopted in this study. The exponential model approximates the empirical semivariogram using the following functional form:

$$\gamma(h) = a\left[1 - \exp(-3h / b)\right] \tag{2.5}$$

where *a* is the *sill* of the semivariogram and also the population variance of random variables, *b* is the *range* of the semivariogram defined as the separation distance *h* at which $\gamma(h)$ equals 95% of the *sill*. In other words, the range *b* is the distance where 95% of correlation is missing. For illustration, an example based on the residuals of CAV from the Chi-Chi earthquake is shown in Fig. 2.1, and the sill and range are marked. If the normalized intra-event residuals are used, they can be computed as:

$$\bar{\varepsilon}_{ij} = \frac{\varepsilon_{ij}}{\sigma_j} \approx \frac{\ln Y_{ij} - \overline{\ln Y_{ij}(M, R, \theta)}}{\sigma_j} \tag{2.6}$$

where $\bar{\varepsilon}_{ij}$ means the normalized residuals, and σ_j is the intra-event standard deviation for site *j* (which can be chosen as either the sample variation from a specific earthquake or the intra-event standard deviation provided by GMPEs). It should be emphasized that Eqn. (2.6) approximates the intra-event residuals using total residuals because the inter-event residual is constant for each site

during one earthquake. Hence, the relationship between the spatial correlation and semivariogram can be simplified as:

$$\rho_{\varepsilon}(h) = \exp(-3h/b) \tag{2.7}$$

Therefore, the range b is the only unknown parameter to quantify the spatial correlation. Several approaches have been proposed in previous studies to fit the empirical data using the exponential model, such as the weighted-least-square method and the manual fitting method. Since it is more important to fit the data at the short distance range, the manual fitting method proposed by Jayaram and Baker (2009) is employed in this study although this approach is relatively subjective.

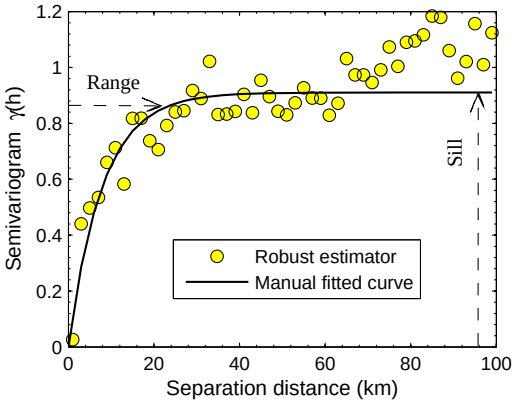

Figure 2.1 An example of empirical semivariograms using robust estimator based on the normalized intra-event residuals of CAV.

2.3. Strong motion database

A total of 1588 ground motion recordings from nine earthquakes are compiled and used to calculate the spatial correlations. These earthquakes occurred in California (1994 Northridge earthquake, 2004 Parkfield earthquake, 2005 Anza earthquake, 2007 Alum Rock earthquake and 2008 Chino Hills earthquake), in Japan (2000 Tottori earthquake, 2004 Niigata earthquake and 2007 Chuetsu earthquake) and in Taiwan region (1999 Chichi earthquake). The time histories for these events are obtained from CESMD (http://strongmotioncenter.org/), CESMOS (http://www.cosmos-eq.org/) for US earthquakes and K-NET (http://www.k-net.bosai.go.jp/) for Japan earthquakes. The seismic information and station conditions are obtained from the Pacific Earthquake Engineering Research (PEER) Center's NGA database (http:peer.berkeley.edu/products/strong_ground_motion_db.html) and the Table S1 database provided by Kaklamanos and Baise (2011).

3. CORRELATION RESULTS

Following the procedures illustrated in the previous section, the normalized intra-event residuals from each earthquake are used to compute the range b of its semivariogram. The shear wave velocity in the top 30 m, V_{s30}, is chosen as an index of the local site condition. The spatial correlation of V_{s30} is quantified using the corresponding semivariograms of the normalized V_{s30} values.

3.1. Spatial correlations of CAV and Ia

Before proceeding, the distribution of the intra-event residuals is examined against the rupture distance to see whether the data exhibit significant bias in distance scaling. The step is essential because it is

possible that the residuals from some events might exhibit systematical bias against the distance, especially for these events that are not used to develop the GMPEs.

Fig. 3.1 plots the distribution of the intra-event residuals against the rupture distance for different earthquakes. These plots clearly show that the biased trends are significant for events out of the NGA database (e.g., all events except for the Chi-Chi and Northridge earthquake), which will result in artificial correlation due to systematical predictive biases in the distance scaling. A simple linear regressed line is also plotted on each subplot.

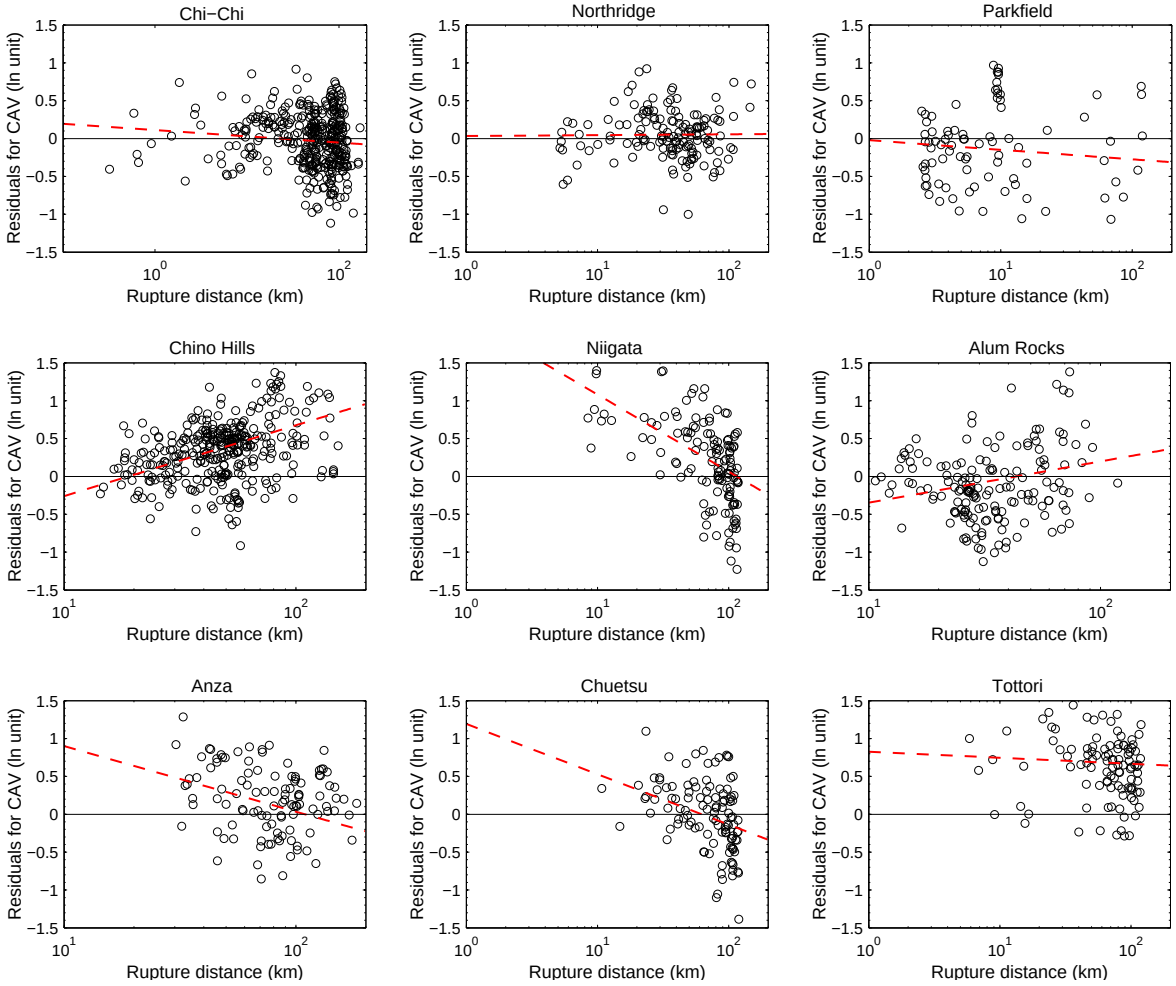

Figure 3.1. Distributions for residuals with respect to rupture distance (km) for nine earthquakes.

It is to be noted that presently no predictive equation for CAV and Ia is available to incorporate these events that are out of the NGA database. Therefore, in order to reduce artificial correlations, an additional distance term is added for each event to correct the intra-event residuals as follows:

$$\varepsilon_{corr} = \ln Y_{ij} - \overline{\ln Y_{ij}\left(M, R, \theta\right)} - \left(\varphi_1 + \varphi_2 \ln(R_{ij})\right) \tag{3.1}$$

where R_{ij} is the rupture distance of the j_{th} recording and i_{th} event, and φ_1, φ_2 are the coefficients obtained by simple linear regression. After this correction to the distance scaling, the residuals show no significant bias against rupture distance for events. For event within the NGA database, such as the Northridge earthquake, the biased trend is not obvious, which implies that residuals for these events can be used directly to compute semivariograms.

After checking the distribution of the residuals, as we mentioned before, the second step is to normalize the intra-event residuals (obtained by logarithm IMs minus logarithm predicted median values). Because only two earthquakes (Northridge and Chi-Chi earthquake) are selected as part of the NGA database to develop GMPEs, it is not surprising that other earthquakes' sample variations are somewhat different from these provided by GMPEs. In view of this, we use the event-specific sample variance rather than these provided by GMPEs. Based on the total number of sites and separation distance of all sites for each earthquake, the width of distance bins varies from 2 km to 6 km for different events to ensure at least 30 pairs of data in each bin.

The empirical semivariograms and the fitted curves for CAV and Ia are shown in Fig. 3.2. All manual fitted curves perform reasonably well at the short distance range, which is the most concerned and important region as was discussed before. For different events, the shape of empirical semivariogram and fitted curves differs significantly. The computed values of range *b* are compiled in Table 3.1. The considerable difference in range *b* implies that the spatial effects of IMs may be influenced by characteristics of different regions, such as the regional geological conditions.

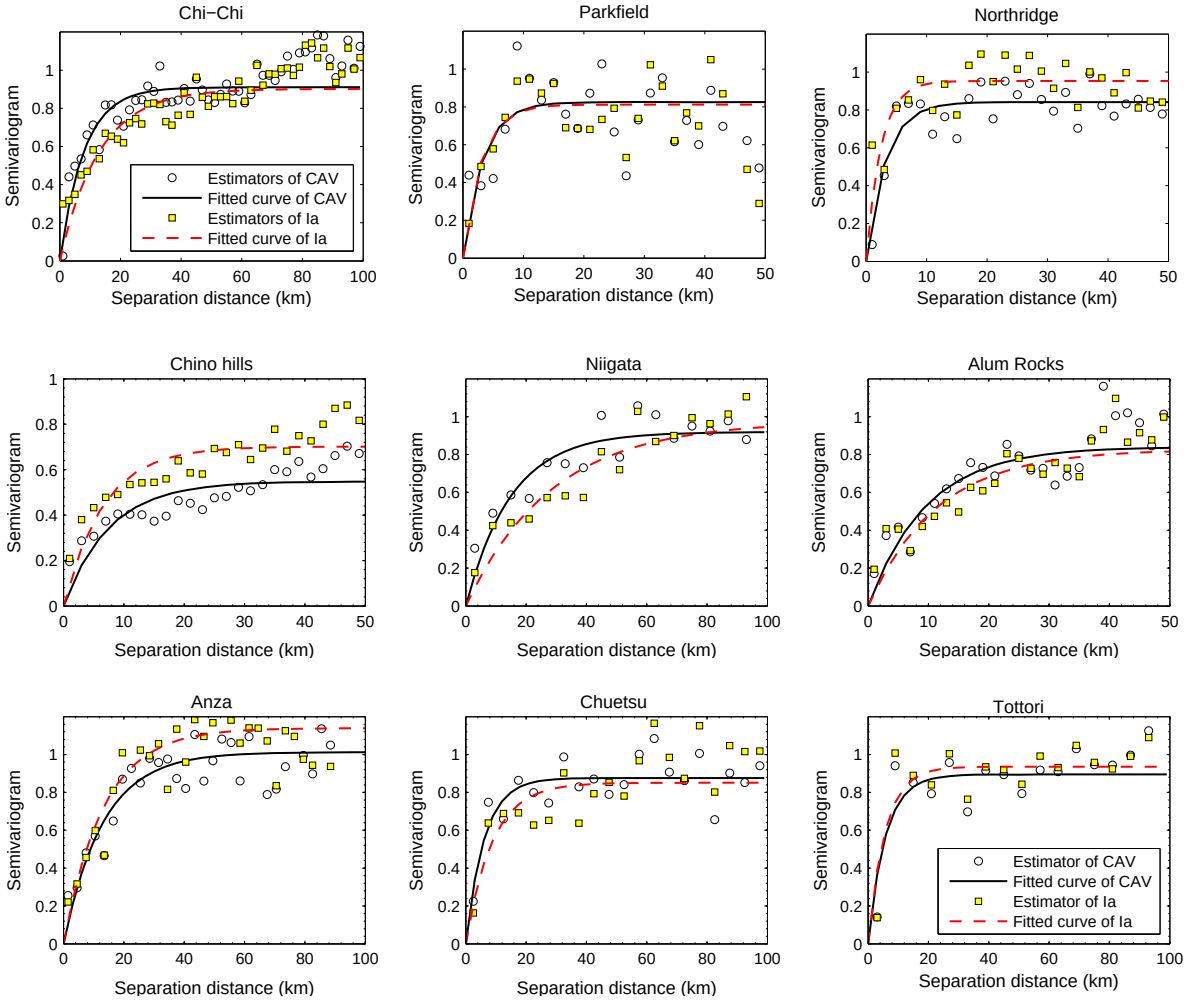

Figure 3.2. Experimental semivariogram obtained by CAV and Ia residuals for nine earthquakes.

3.2. Spatial Correlations of V_{s30}

Due to the fact that the travel path and frequency contents of earthquake waves are strongly dependent on the local geology condition, the effects of local geological conditions on the spatial IM correlation have been investigated (e.g. Jayaram and Baker, 2009). For this purpose, the correlation range of the normalized V_{s30} values (normalized by the averaged V_{s30}) can be used to represent the homogeneity of

the regional geological conditions, as a larger correlation range of the V_{s30} simply implies a more uniform geological condition. One can refer to Jayaram and Baker (2009) for more details.

However, most V_{s30} values in the strong motion database are not directly measured but inferred from other geological information. In this regards, a constant V_{s30} value is often assigned to sites that are identified as being in the same site category. The inference results in reduced variability of the V_{s30} distribution compared with the variability of measured data for some regions. These inferred V_{s30} values tend to imply a more uniform geological condition than the actual case, and consequently, an artificially increased spatial correlation range of V_{s30}. Even for well-recorded events such as the Chi-Chi or Northridge earthquake, the number of measured V_{s30} values is less than 40% of the total data. In addition, only approximately 5% of measured V_{s30} values are available for the Anza and Chino Hills earthquakes. Figure 3.3(a) displays the distribution of V_{s30} values against the rupture distance for Chino Hills event, where a large number of identical V_{s30} values are inferred. As is explained previously, the situation could greatly increase the range of spatial correlation for V_{s30}.

A simple correction method is implemented to reduce the fake spatial correlations of V_{s30}. Firstly, all V_{s30} data are randomly re-distributed around that value using Monte-Carlo method by assuming V_{s30} follows a lognormal distribution with a specific standard deviation. The standard deviation of $\ln V_{s30}$ is assumed to be 0.2 for measured data 0.3 for inferred data, as was provided by Chiou *et al.* (2008). Figure 3.3(b) displays one realization of the randomly redistributed V_{s30} values. Secondly, the Monte-Carlo simulations are repeated for two thousand times and the value of range *b* is obtained for each realization. Finally, we choose the mean value of the computed *b* as the corrected range of (normalized) V_{s30}. After this correction, the correlation ranges of V_{s30} for some events are greatly reduced as expected. For instance, the V_{s30} range for the Chino Hills event is reduced from 35 km to 14.7 km after correction. The corrected V_{s30} ranges for nine aforementioned earthquakes are also listed in Table 3.1.

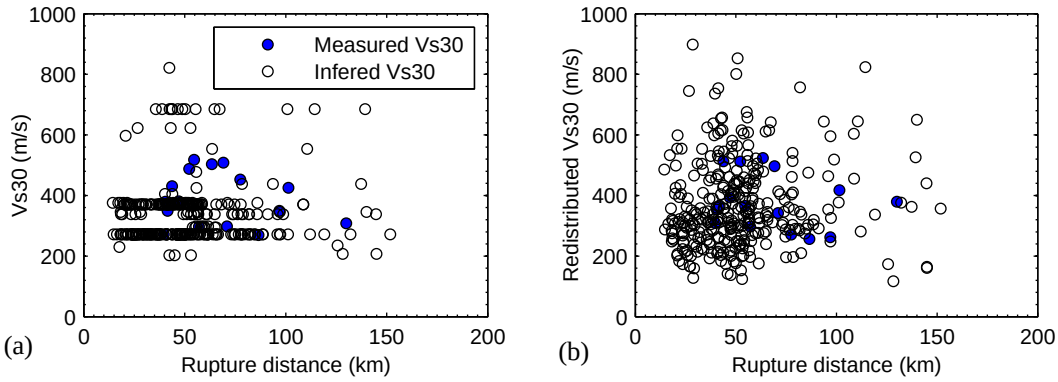

Figure 3.3. (a) Distribution of V_{s30} values and (b) redistributed V_{s30} values with respect to rupture distance (km) for Chino hills earthquake.

Table 3.1. Values of range *b* (in km) for CAV, Ia, PGA and V_{s30}

Events	CAV	Ia	PGA	V_{s30}	Events	CAV	Ia	PGA	V_{s30}
Northridge	11	7.4	10.8	0	Chi-Chi	24	38	48	27.7
Parkfield	10	9.2	7.6	2.9	Tottori	19.3	16.7	20.6	18.7
Anza	42	35.6	54	20.3	Niigata	29.7	32	54	22.3
Alum Rock	27.4	34	21.5	13.7	Chuetsu	18	19	22	21.2
Chino Hills	20.3	19.8	16	14.7					

3.3. Predictive models based on site conditions

In this subsection, relationships between the ranges of IMs (CAV, Ia and PGA) with that of V_{s30} values are examined. As is shown in Figure 3.4, the ranges of IMs are in general positively correlated with the range of V_{s30}. i.e., the correlation range of an IM increases if the range of V_{s30} values increases (more homogeneous). For practical purpose, three simple fitting functions are provided as follows:

$$\text{CAV:}\quad b_{CAV} = 11.65 + 0.68 b_{vs} \qquad (\sigma=8.2) \tag{3.2}$$

$$\text{Ia:}\quad b_{Ia} = 7.92 + b_{vs} \qquad (\sigma=7.8) \tag{3.3}$$

$$\text{PGA:}\quad b_{PGA} = 8.92 \exp(0.065 b_{vs}) \qquad (\sigma=12.2) \tag{3.4}$$

where b_{vs}, b_{CAV}, b_{Ia}, b_{PGA} represent the correlation range related to the normalized V_{s30} and the normalized IM (CAV, Ia, PGA) residuals, respectively. As is shown in Fig. 3.4, the predictive model shows reasonably good agreement with the emprical data. The standard deviations σ of the predicted *b* values are also provided in Eqs. (3.2)-(3.4) to quantify the uncertainty associated with the estimation. It is observed that the ranges of spatial correlations for CAV, Ia and PGA are similar if the range of V_{s30} is small (the site condition is more heterogeneous), while the difference becomes more pronounced when the range of V_{s30} increases (the site condition is more homogeneous). In general, Ia have slightly larger correlation range than that of CAV. For a relatively homogeneous geological condition, PGA appears to have a stronger spatial correlation (i.e., a larger correlation range) than CAV and Ia. For example, if the range of the normalized V_{s30} is 20 km, the predicted range for CAV, Ia and PGA are 25 km, 27.9 km and 32.7 km, respectively.

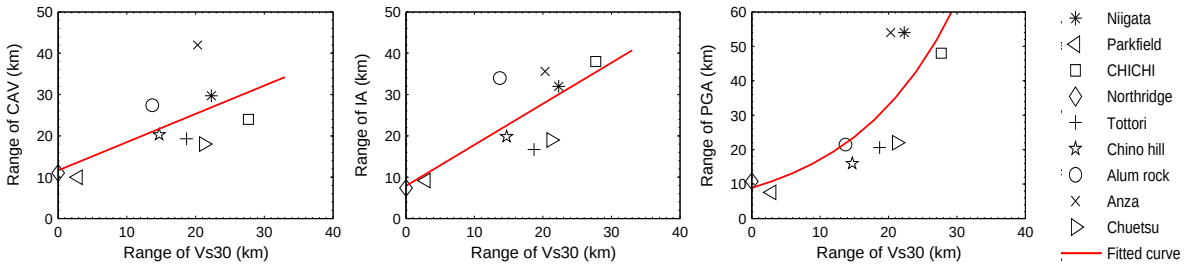

Figure 3.4. Ranges of residuals calculated by IMs (CAV, Ia and PGA) with respect to normalized V_{s30} values.

4. CONCLUSIONS AND DISCUSSIONS

In this paper, the spatial correlations of Ia and CAV are obtained by semi-empirical estimation using nine recent earthquakes. An exponential model is used to represent the spatial correlation as a function of the separation distance. The ranges of normalized V_{s30} values are computed as an index to represent the homogeneity of the local site condition. Correction methods are applied to reduce artificial correlation arising from biased predictive models or inferred V_{s30} values. The results indicate that, the spatial correlations for IMs (CAV, Ia and PGA) are strongly dependent on the local site conditions. Hence, some simple equations are proposed to quantify the spatial correlations of IMs with respect to the range of V_{s30} values. For a specific region, firstly we estimate the range of V_{s30} values based on geological information of neighboring sites. Then, the correlation range of IMs can be easily evaluated for further risk assessment and loss estimation.

In previous sections, particular GMPEs are chosen to predict the intensity measures, so the results might be influenced by the choice of GMPEs. We also used other GMPEs for CAV and Ia available in literature to obtain the empirical semivariograms. Very similar results can be derived by using different GMPEs, indicating that obtained spatial correlation is model independent. A previous study (Piggott and Stafford, 2011) on the correlation model for Ia (using the Chi-Chi and Northridge

earthquake) shows a slightly smaller correlation range than that in the present study. For instance, the reported correlation range for the Chi-Chi earthquake is 31 km in Piggott and Stafford (2011) compared with 38 km in this study. The difference can be attributed to epistemic uncertainty using different GMPEs and fitting technique. There is no comparable result related to the spatial correlation of CAV in literature.

Finally, an illustrative example is provided to highlight the importance of the spatial correlation of IMs in seismic hazard analysis. Considering a hypothetical region 40 km × 40 km in size located near a point source at the origin, the area is divided into cells of 1km × 1 km in size. Assuming that the style of faulting is a reverse fault, the average site conditions of the region is deep soils (the averaged V_{s30}=240 m/s). For illustration purposes, a scenario earthquake with moment magnitude of 7 and corresponding annual exceedance rate of $\lambda_M = 1/500$ is considered. GMPE (i.e., Campbell and Bozorgnia, 2012) provides the predicted median and the standard deviation of Ia values at each site location. Copula functions (Nelson, 2006) can be used to generate the intra-event residuals, which are normally distributed with a zero mean and a standard deviation specified by GMPEs at each site, while at the same time, they are spatially correlated according to the given spatial correlation coefficients. Detailed procedures can be found in the references (e.g. Sokolov and Wenzel, 2011). Two Monte Carlo realizations of Ia values (in natural log scale) are shown in Figure 4.1 by assuming the correlation ranges of 10 km and 40 km, respectively. As is expected, a large correlation range corresponds to a more uniform spatial distribution of Ia's, as shown in Fig. 4.1(b).

Monte Carlo method is applied to generate 10000 realizations of spatially-correlated Ia values over the region. Given a specified value of Ia (denoted as Ia^*) and its exceedance area ratio AR^* (defined as ratio of the areas whose Ia values exceed the specified Ia^* value against the total area of the region), the annual rate of exceedance can be computed from the Monte Carlo realizations as:

$$\lambda = \lambda_M \cdot P(Ia > Ia^* \,\&\, AR > AR^*) \tag{4.1}$$

Several special cases are considered for comparison by assuming that the intra-event residuals of Ia are independently distributed without spatial correlation (correlation range is zero), or spatially correlated with the correlation range of 10 km and 40 km, respectively; or perfectly correlated (correlation range is infinite such that the residuals are identical over the region). Figure 4.2 shows the annual exceedance curve for Ia with the exceedance area AR^* of 5% and 25%, respectively. The results imply that, the spatial correlation does increase the probability of rare occurrence of the IM, especially when the mean annual rate of exceedance is smaller than 10^{-4} in our case. For example, given an annual rate value 10^{-4}, the predicted Ia values for 25% area of exceedance for uncorrelated case and correlated case (range of 40 km) is 1.06 m/s and 1.45 m/s, respectively. So the hazard is underestimated if no correlation is assumed.

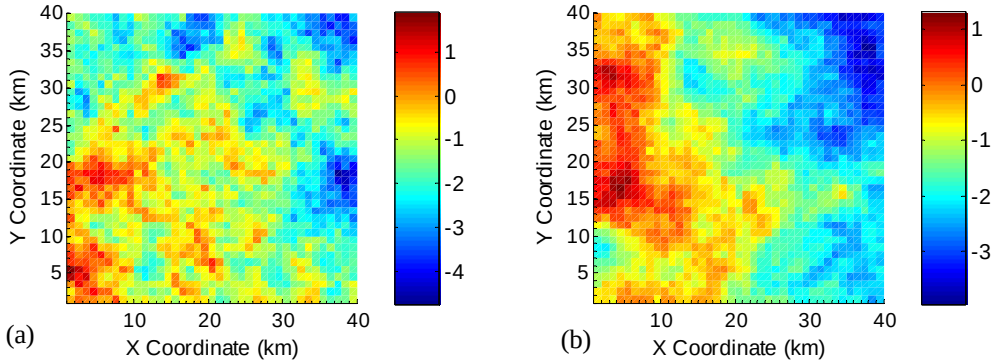

Figure 4.1. Examples of realized spatially-correlated field of Ia (in natural log scale, unit of m/s) (a) correlation range as 10 km and (b) correlation range as 40 km.

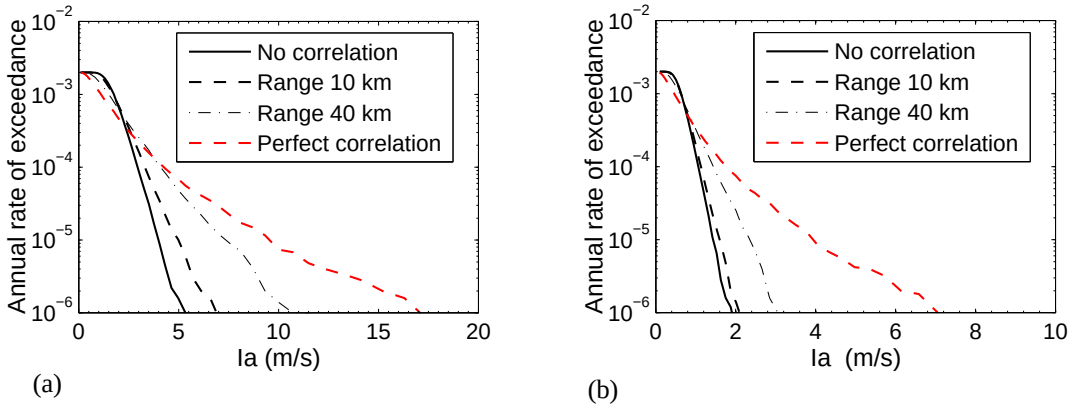

Figure 4.2. Annual exceedance hazard curves for Ia considering different spatial correlations for (a) exceedance area ratio AR^* as 5% (b) as 25%

AKCNOWLEDGEMENT

The research is supported by Hong Kong Research Grants Council (grant No. 620311), which is greatly acknowledged.

REFERENCES

Abrahamson, N.A., Youngs, R.R. (1992). A stable algorithm for regression analyses using the random effects model. *Bulletin of the Seismological Society of America* **82**, 505-510.

Arias, A. (1970). Measure of earthquake intensity. Seismic design for nuclear power plants, 438-483.

Boore, D.M., Gibbs, J.F., Joyner, W.B., Tinsley, J.C., Ponti, D.J. (2003). Estimated ground motion from the 1994 Northridge, California, earthquakes at the site of the Interstate 10 and La Cienega Boulevard bridge collapse, West Los Angeles, California. *Bulletin of the Seismological Society of America* **93:6**, 2737-2751.

Campbell, K.W., Bozorgnia, Y. (2010). A ground motion prediction equation for the horizontal component of cumulative absolute velocity (CAV) based on the PEER-NGA strong motion database. *Earthquake Spectra* **26:3**, 635–650.

Campbell, K.W., Bozorgnia, Y. (2012) A comparison of ground motion prediction equations for Arias intensity and cumulative absolute velocity developed using a consistent database and functional form. *Earthquake Spectra*, in press.

Chiou, B. S.-J., Darragh, R., Gregor, N., and Silva, W. (2008). NGA project strong-motion database. *Earthquake spectra* **24**, 23–44.

Cressie, N. (1993). Statistics for Spatial Data, Revised edition. Wiley, New York.

Cressie, N. and Hawkins, D.M. (1980). Robust estimation of variogram. *Mathematical Geology* **12:2**, 115–125.

Electrical Power Research Institute (EPRI) (1988). A criterion for determining exceedance of the operating basis earthquake, Report No. EPRI NP-5930, Palo Alto, California.

Esposito, S., Iervolino, I. (2011). PGA and PGV spatial correlation models based on European multievent datasets. *Bulletin of the Seismological Society of America* **101:5**, 2532-2541.

Goda, K., Atkinson, G.M. (2010). Intraevent spatial correlation of ground-motion parameters using SK-net data. *Bulletin of the Seismological Society of America* **100:6**, 3055-3067.

Jayaram, N, Baker, N.J. (2009). Correlation model for spatially distributed ground-motion intensities. *Earthquake Engineering and Structural Dynamics* **38**,1687-1708.

Kaklamanos, J., Baise, L.G. (2011). Model validations and comparisons of the next generation attenuation of ground motions (NGA-West) project. *Bulletin of the Seismological Society of America* **101:1**, 160-175. Table S1 in the electronic supplement.

Nelson, R.B. An introduction to Copulas. (2006). Springer series in statistics. Springer: New York.

Piggott, R.F., Stafford, P.J. (2011). A predictive model for Arias intensity at multiple sites and consideration of spatial correlations. *Earthquake Engineering and Structural Dynamics* **41:3**, 431-451.

Sokolov, V, Wenzel, F. (2011). Influence of spatial correlation of strong ground motion on uncertainty in earthquake loss estimation. *Earthquake Engineering and Structural Dynamics* **40**, 993-1009.